SIMULATION STUDIES ON CHIP FORMATION PROCESS IN HIGH SPEED MILLING OF ALUMINIUM ALLOY

Pham Thi Hoa[1, 2, *], Mac Thi Bich[1, 2], Banh Tien Long[1], Nguyen Duc Toan[1]

[1]*Department of Mechanical Engineering, Hung Yen University of Technology and Education, Dan Tien Ward, Khoai Chau District, Hung Yen Province, Vietnam*

[2]*School of Mechanical Engineering, Hanoi University of Science and Technology, Number 1°, Dai Co Viet Street, Hai Ba Trung District, Hanoi City, Vietnam*

[*]Email*: hoapt2108@gmail.com*

Received: 20 July 2016; Accepted for publication: 3 December 2016

ABSTRACT

Simulations of chip formulation mechanism and phenomenon ccurred in cutting processes can help to reduce time and cost comparing with experiment. Finite element method (FEM) is an effective and accurate technique, which can be used for simulation of cutting process. In this paper, chip formulation process in high-speed milling of A6061 aluminium alloy is investigated using FEM based on the Johnson-Cook (J-C) and Bao-Wierzbicki (B-W) fracture models. The Von-Mises stress distribution and equivalent plastic strain (PEEQ) during cutting are then investigated. Finally, the evolution of cutting forces in cutting was examined. The presented Finite element model in this study proved to be useful in determination of cutting parameters, especially in high-speed machining.

Keywords: high-speed milling, A6061 aluminum alloy, simulation using finite element.

1. INTRODUCTION

Nowadays, high-speed machining has recieved a great deal of attention in morden industrial to achieve high quality and productivity in manufacturing. The chip formation mechanism in high-speed machining is one of the most important factors influencing the surface finish of machining product and other cutting parameters such as cutting force, temperature, vibration, wear and life of cutting tool. There have been a numerous studies conducted using different cutting methods and workpiece materials. Ceretti et al. [1] simulated the continuous and segmented chip formation in relations to cutting speed, rake angle, and depth of cut using a commercial Finite Element (FE) code 2D DEFORM. Strenkowski and Moon [2] predicted the chip geometry and tool/workpiece temperature distributions in orthogonal metal cutting using an Eulerian FE model and validated theri model based on cutting experiments of aluminum alloy 6061-T6. Li et al. [3] simulated the residual stress in high-speed end-milling of hardened steel SKD11 using a two-dimension (2D) thermo-mechanical FE model. They used the Johnson-Cook plasticity model for modeling of the workpiece material. They found that the residual stresses

shows increasing trend, whist the tensile and compressive stresses approach a state of equilibrium. Deng et al. [4] presented a thermo-elastic-plastic FE model to simulate the chip breaking of medium carbon steel AISI1045 with grooved tool based on the normalized Cockcroft & Latham's criterion. From a detailed observation of distributed temperature, cutting force, stress and strain during cutting, they concluded that the cutting force, which varies within a chip breaking cycle, plays an important role for identifying the chip breaking event. Recently, Buchkreme et al. [5] proposed a new FE-modeling approach to predict the relationship between the distribution of the stress triaxiality and 3D chip geometry in turning process of AISI 1045. They highlighted that the stress triaxiality at major cutting edge increases with decreasing chip helical radii. Whereas, the chip helical pitch has a negligible influence on the stress triaxiality. In general, FE model has been effectively used in simulation of chip formation in high-speed machining. The FEM is capable of providing more detailed information of cutting process than those of experiments, reducing the computational efforts and flexible for different cutting conditions or work-piece materials.

In this study, the FEM is developed to simulate the chip formation during milling of A6061 aluminium alloy. The 3D FE modeling was peformed using the ABAQUS 6.13 commercial software. Two material fracture models e.g., Johnson-Cook (J-C) and Bao-Wierzbicki (B-W) were used to describe the fracture criteria for the workpiece material. The stress and strain of chip and cutting force in milling process were also investigated.

2. MATERIAL FRACTURE MODELS

2.1. Strain coefficient and fracture point

In a chip formation process, there exists a equivalent strain to fracture ε_f^{-pl}, at which the fracture occurs. Then, the material is damaged according to following condition [6]:

$$\varepsilon^{-pl} \geq \varepsilon_f^{-pl} \tag{1}$$

where ε^{-pl} is the equivalent strain.

From the criterion in Eq. (1), there are several fracture models those describe the fracture of material as follows:

2.1.1. The Johnson- Cook (J-C) model

The J-C fracture model states that fracture occurs when the accumulated plastic strain reaches a critical value. The damage parameter (D) is determined by

$$D = \sum \frac{\Delta\varepsilon^{-pl}}{\varepsilon_f^{-pl}} \tag{2}$$

where $\Delta\varepsilon^{-pl}$ indicates the equivalent plastic strain-rate. ε_f^{-pl} is the equivalent strain to fracture, calculated by:

$$\varepsilon_f^{-pl} = [D_1 + D_2 \exp(D_3\eta)][1 + D_4 \ln\left(\frac{\bar{\dot{\varepsilon}}^{pl}}{\dot{\varepsilon}_0}\right)] \tag{3}$$

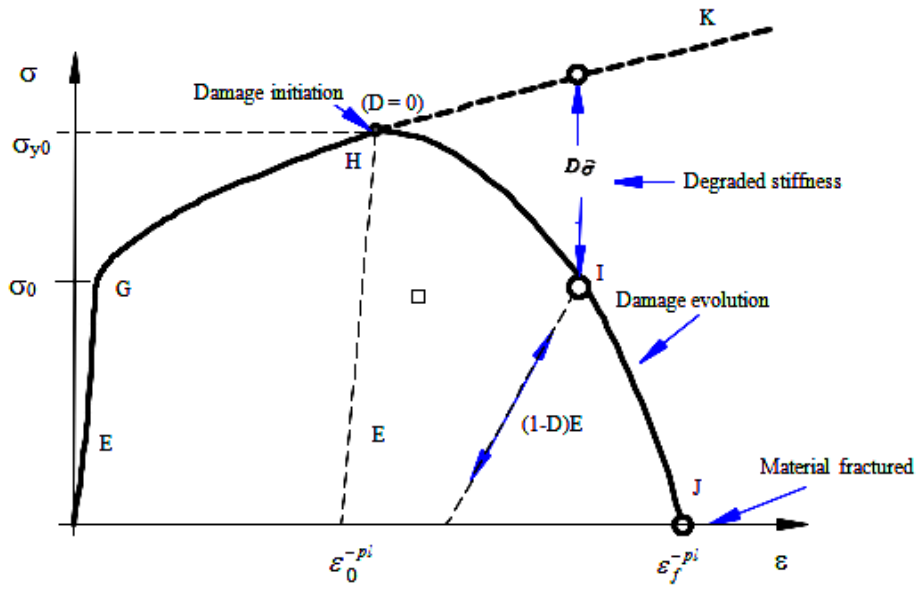

Figure 1. Uniaxial stress–strain curve of a metal specimen [6].

where $D_1...D_4$ are dimensionless fracture constants determined by experiment. η represents the stress triaxiality parameter $\eta = \frac{p}{q}$, where p is the average of the three normal stresses. q is the Von-Mises equivalent stress. Then can η be calculated by:

$$\eta = \frac{\frac{\sigma_1 + \sigma_2 + \sigma_3}{3}}{\sqrt{\frac{1}{2}\left[(\sigma_1 - \sigma_2)^2 + (\sigma_3 - \sigma_2)^2 + (\sigma_1 - \sigma_3)^2\right]}} \tag{4}$$

where σ_1, σ_2 and σ_3 are the normal stresses components.

The typical uniaxial stress-strain curve of a ductile metal is demonstrated in Figure 1. It comprises of the initially linear elastic region (F-G), plastic yielding region with strain hardening (G-H), neck region (H-J) with a fracture point J. Beyond point H the load-carrying capacity starts to reduce until fracture. Point H is defined as the damage initiation criterion of material. In the neck region, the localized stiffness degradation is occurred. In view damage mechanics, a period without damage may be expected (H-K). The chip formation process involves two steps: damage initiation and damage evolution [7].

2.1.2. The Bao-Wierzbicki (B-W) fracture model

The B-W fracture model indicates that the fracture occurs when the accumulated plastic strain reaches a critical value. The damage parameter is calculated by [10]

$$D = \int_0^{\bar{\varepsilon}_f} \frac{\sigma_H}{\bar{\sigma}} d\bar{\varepsilon} = \left(\frac{\sigma_H}{\bar{\sigma}}\right)_{av} \bar{\varepsilon}_f \tag{5}$$

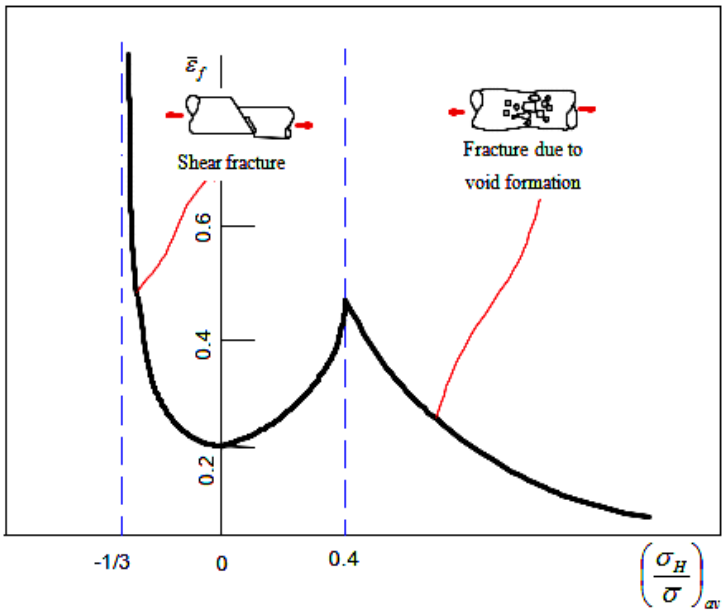

Figure 2. Fracture curve of material based on the B-W model [9].

where D is accumulated equivalent plastic strain. $\left(\frac{\sigma_H}{\bar{\sigma}}\right)_{av}$ is the average stress triaxiality. $\bar{\varepsilon}_f$ represents the equivalent strain to fracture. Figure 2 shows an example of the equivalent strain to fracture dependent on the average stress triaxiality in which the equivalent strain to fracture is expressed by following curve-fitting formulae [8, 9]

$$\bar{\varepsilon}_f = \begin{cases} 0.1225\left(\frac{\bar{\sigma}_H}{\bar{\sigma}}+\frac{1}{3}\right)^{-0.48} & for \quad \frac{\bar{\sigma}_H}{\sigma} = -\frac{1}{3}-0 \\ 1.9\left(\frac{\bar{\sigma}_H}{\bar{\sigma}}\right)^2 - 0.18\left(\frac{\sigma_H}{\bar{\sigma}}\right)+0.21 & for \quad \frac{\bar{\sigma}_H}{\sigma} = 0-0.4 \\ 0.15\left(\frac{\bar{\sigma}_H}{\bar{\sigma}}\right)^{-1} & for \quad \frac{\bar{\sigma}_H}{\sigma} = 0.4-0.95 \end{cases} \tag{6}$$

Figure 3 shows the variation of the equivalent strain to fracture using the J-C and B-W mode, i.e., equation (3) and (6), respectively. From Figure 3, one can see the differences between the equivalent strain calculated by the two fracture models. Using the B-W mode, the highest point of 0.4 can be observed.

2.2. Mechanical properties of Aluminium alloy A6061

In this study, the workpiece material of aluminium alloy A6061 is used. This material is widely used in industrial because of its excellent properties regarding wear resistance, weldability and strength. Major chemical compositions and physical properties of A6061 aluminum alloy are shown in Tables 1 and 2, repectively. Table 3 shows the material constants according to the J-C model.

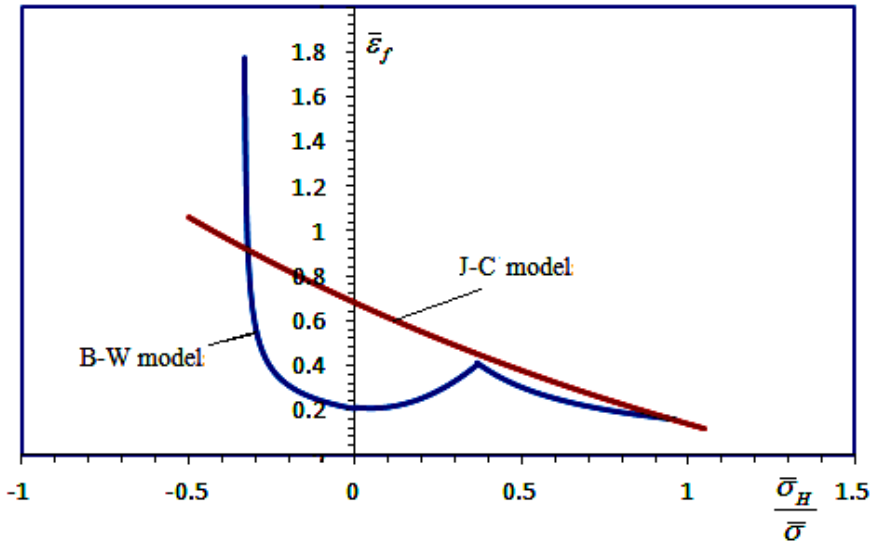

Figure 3. The equivalent strain to fracture $\bar{\varepsilon}_f$ based on the J-C and B-W models.

Table 1. Chemical composition of A6061 aluminum alloy (%).

Si	Fe	Cu	Mn	Mg	Cr	Zn	Ti	Al
0.4-0.8	0.7	0.15-0.4	0.15	0.8-1.2	0.04-0.35	0.25	0.15	remaining

Table 2. Physical properties of A6061 aluminum alloy.

Physical properties	*Value*	*Physical properties*	*Value*
Melt temperature (^{0}C)	582-652	Elastic modulus (Gpa)	68.9
Thermal conductivity coefficient (W/m.K)	167	Resistance (Ω.m)	3.99e-006
Specific heat capacity (J/g^{0}C)	0.896	Fracture strength (Mpa)	96.5
Density (kg/m^3)	2.7	Tensile strength (Mpa)	276
Hardness (HB)	95	Poisson's ratio	0.33

3. SIMULATION DESIGN

3.1. Simulation model

In this study, the Abqus/Explicit 6.13 commercial software will be used for simulation of chip formation in milling of A6061 aluminum alloy. Figure 4 shows the 3D model and boundary conditions of the cutting tool and workpiece. Simulation is performed for 1/4 of circular workpiece with 60 mm in diameter, and 20 mm in thickness (Figure 4). All six degrees of freedom (DOF) of the workpiece and five DOF of the cutting tool are fixed. Thus, the only motion of the tool is rotational motion around Z axis. To archive the generated chip with desired thickness, the workpiece is devided into 3 parts as shown in Figure 5. Part 1 represents the uncut

chip portion, which forms the major part of the chip. Thickness of part 1 is equal to feed rate of 0.135 mm. Part 2 is the sacrificial layer of 0.1 mm thickness. This part directly interacts with cuttingtool leading the fracture of the mesh element. The elements in the sacrificial layer will be removed if they are completely damaged. Otherwise, they will be added to the uncut chip portion to form the produced chip. Parts 1 and 2 have a thickness of 1 mm equal to cutting depth. Part 3 indicates the remaining portion of cutting tool radius contacting to the workpiece. This part consists of the mesh elements, which will not be damaged during simulation. The remaining portion of workpiece is part 4. The mesh size of elements in part 4 is relatively higher than those of other parts. Simulation will be performed for a cutting speed of 1256 m/min, depth of cut of 1 mm and feed rate per revolution of 0.135 mm. The rake angle and plane approach angle of cutting tool are 0° and 10°, respectively.

Table 3. Material constant based on the J-C model.

D1	D2	D3	D4	D5
-0.77	1.45	-0.47	0.0	1.60

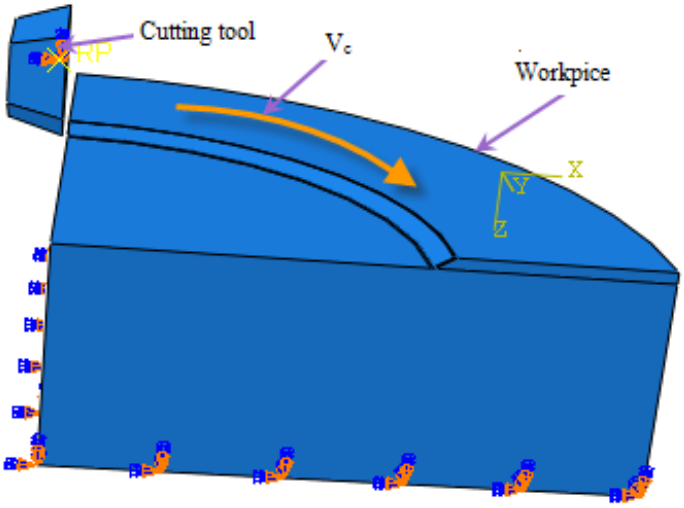

Figure 4. Boundary conditions of workpiece and cutting tool.

3.2. Stress distribution at the tool-chip interface

In the cutting process, stresses developed in the cutting regions should be reduced to avoid cracks on the machined surface. The fracture criteria of material are assumed identical for compression, tension, shear, and other loading conditions. There are three stages of chip formation. In the first tool cut-in stage, the cutting tool touches the workpiece. In the second chip generation stage, the formation of chip is beginning. The third stage is chip formation stage.

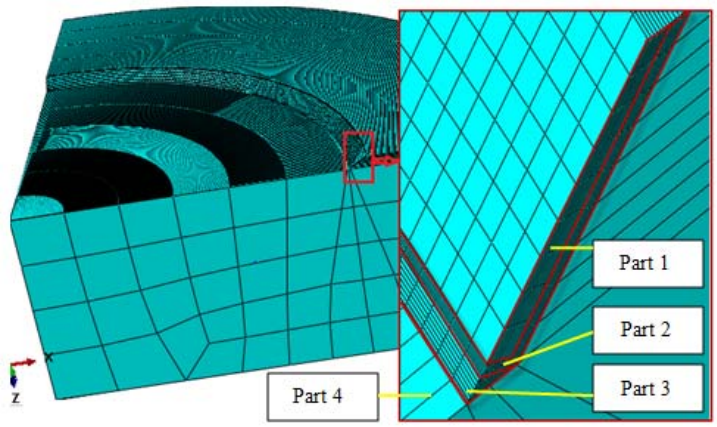

Figure 5. Finite element model.

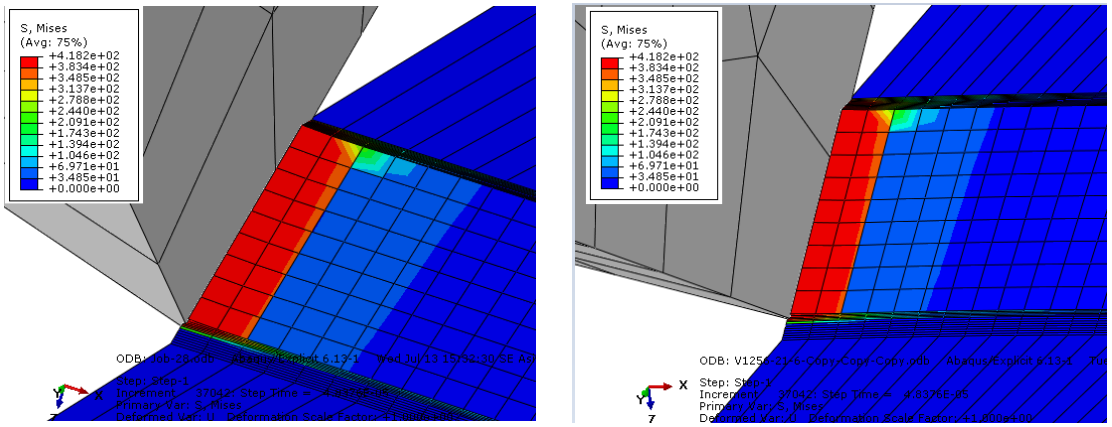

a) b)

Figure 6. Von-Mises stress in the first stage of chip formation, (a) the J-C model, (b) the B-W model.

Figures 6, 7 and 8 describe the simulated Von-Mises stress at the tool-chip interface in the above-mentioned stages by using the J-C and B-W models. The concentrated stresses around the tool-chip contact regions are very high and gradually increase with cutting stage. The stresses predicted by the J-C model are a little lower than those estimated by the B-W model for the second and third stages. Whereas there is no difference in the Von-Mises tresses estimated by the two models in the tool cut-in stage. Maximum difference occurred at the second and third stages are 10.84 % and 5.37 %, respectively.

Figures 9 and 10 show the equivalent plastic strain (PEEQ) of chip by using the J-C and B-W models, respectively. In the second and third stages, PEEQ estimated by the B-W model is higher than using the J-C model as shown in Figures. 9 and 10. On contrary, PEEQ using B-W is smaller in the first stage.

In the first stage, a localized deformation zone forms in front of the tool tip with relatively low maximum PEEQ. As the cutting growing, continuous chips are formed due to ductility property of the workpiece material. PEEQ increases significantly and spreads along the produced chip.

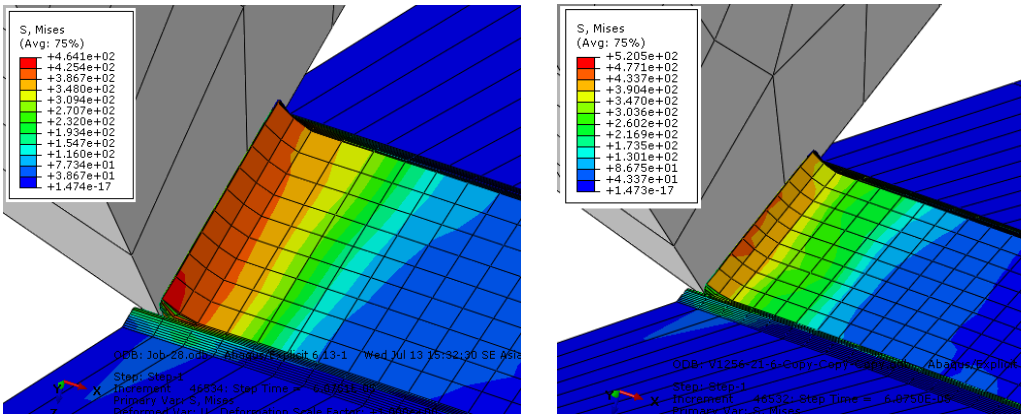

a) b)

Figure 7. Von-Mises stress in the second stage of chip formation, (a) the J-C model, (b) the B-W model.

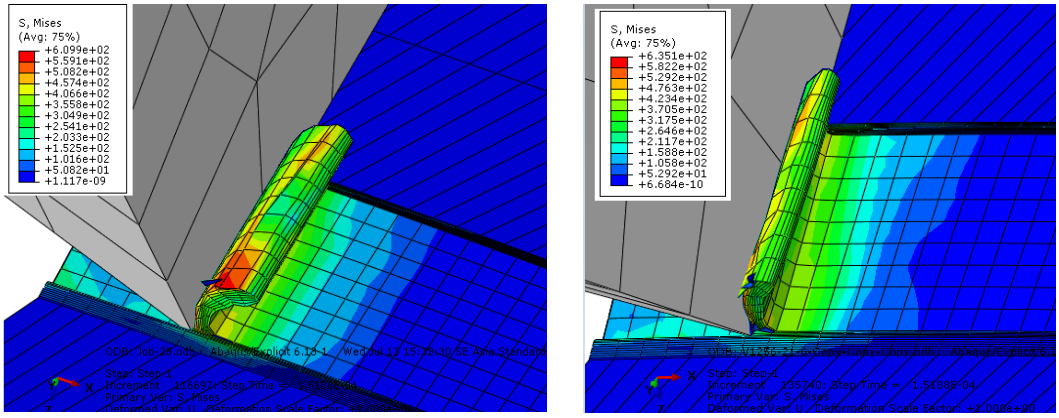

a) b)

Figure 8. Von-Mises stress in the third stage of chip formation, (a) the J-C model, (b) the B-W model.

3.3. Prediction of cutting forces

Cutting force is important for predicting other behaviors of cutting process for example, stress developing, temperature growth, etc. Besides, it is also used for evaluating the energy consumption of cutting [10]. During a cutting process, the cutting force also influences the tool performance such as lifetime, vibration, and wear. During simulation by FEM, the generated cutting force comprises of three elementary forces F_x, F_y, F_z. The resultant force is obtained by

$$F = \sqrt{F_x^2 + F_y^2 + F_y^2} \tag{7}$$

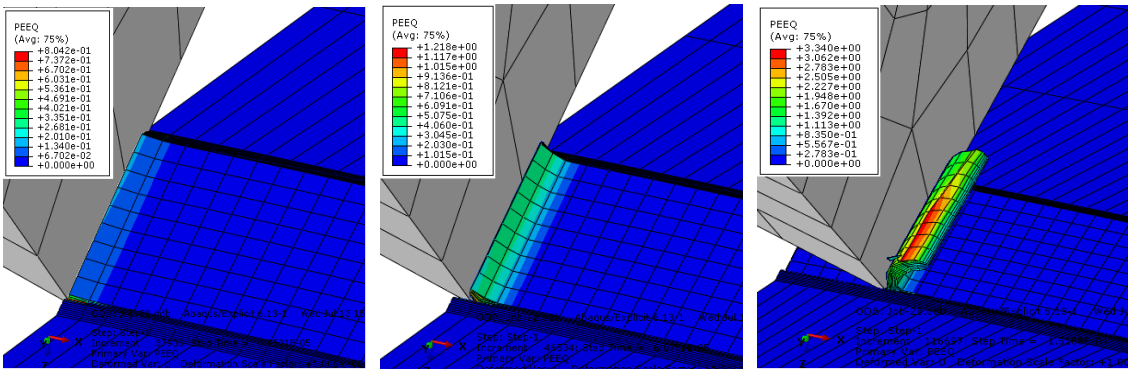

a) b) c)

Figure 9. Equivalent plastic strain using the J-C model, (a) First stage, (b) Second stage, (c) Third stage.

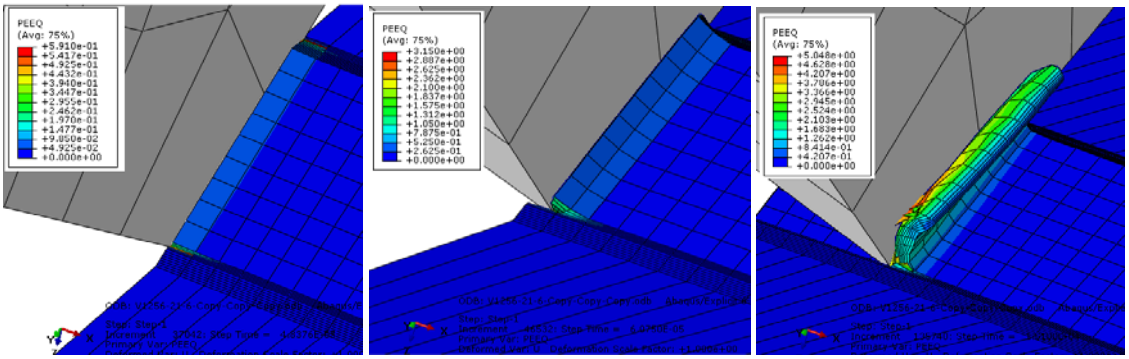

a) b) c)

Figure 10. Equivalent plastic strain using the B-W model, (a) First stage,(b) Second stage,(c) Third stage.

Figure 11 shows the simulation results of time-varying cutting forces by the J-C, B-W. Generally, the cutting forces gradually increase so as the PEEQ and Von-Mises stress (Figures 8-11). With the same mesh size FE model, fluctuation range of the force based on the B-W model is lower than those based on the J-C model. In other words, the cutting force simulated using the B-W model is more stable.

The results in Figure 11 also shows that the average value of the cutting force of J-C model higher than B-W model as shown in the dotted trendlines. This is because the fracture point in the B-W model is lower than in the J-C model as shown in Figure 3.

4. CONCLUSION

FE simulation for high-speed milling of A6061 aluminum alloy has been performed. The FE model was created based on two fracture models: the J-C and the B-W models. The evolution of stress distribution and PEEQ are investigated in correspondence with three stages of cutting process. The presented model in this paper is beneficial of providing detailed stress and deformation during cutting, which are hard to obtain by experimental measurement, especially in high-speed machining. The current model in this paper can be further extended to predict the other parameter in machining, especially in high-speed cutting.

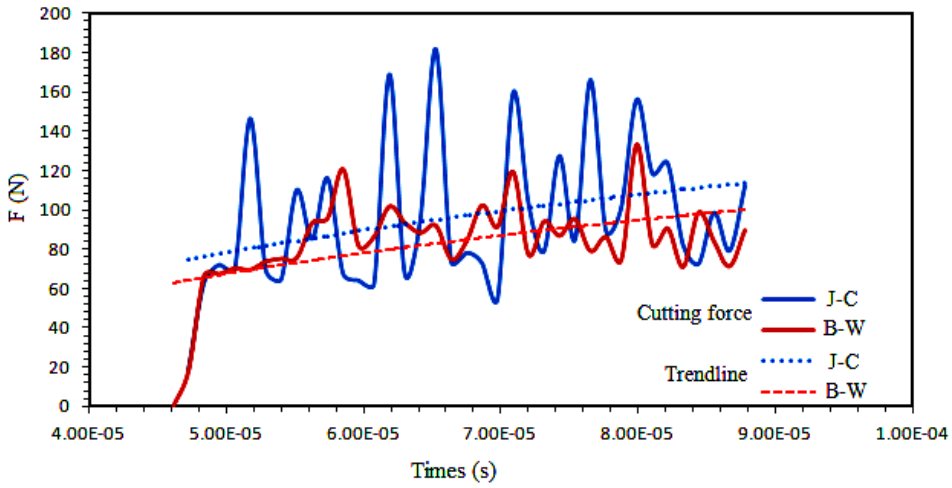

Figure 11. Simulation cutting force.

REFERENCES

1. Ceretti E, Fallböhmer P, Wu W. T, and Altan T. - Application of 2D FEM to chip formation in orthogonal cutting. J. Mater. Process. Technol. **59** (1–2) **(**1996) pp. 169–180.
2. Strenkowski J. S. and Moon K.J. - Finite Element Prediction of Chip Geometry and Tool/Workpiece Temperature Distributions in Orthogonal Metal Cutting. J. Eng. Ind **112** (4) (1990) p. 313.
3. Li J. L, Jing, L. L. and Chen M. - An FEM study on residual stresses induced by high-speed end-milling of hardened steel SKD11. J. Mater. Process. Technol. **209** (9) **(**2009) pp. 4515–452.
4. Deng W. J, Xie C. Z, Li Q, and Lin P. - Finite element modelling and simulation of chip breaking with grooved tool. Int. J. Simul. Model. **12** (4) **(**2013) pp. 264–275.
5. Buchkremer S, Klocke F, and Veselovac D, - 3D FEM simulation of chip breakage in metal cutting, Int. J. Adv. Manuf. Technol. **82** (1–4) (2016) pp. 645–661.
6. Liu J, Bai Y, and Xu C. - Evaluation of Ductile Fracture Models in Finite Element Simulation of Metal Cutting Processes. J. Manuf. Sci. Eng. **136 (**2013) p. 011010.
7. Mabrouki T, Girardin F, Asad M, and Rigal J. F. - Numerical and experimental study of dry cutting for an aeronautic aluminium alloy (A2024-T351). Int. J. Mach. Tools Manuf. **48** (11) (2008) pp. 1187–1197.
8. Bao Y. and Wierzbicki T. - On fracture locus in the equivalent strain and stress triaxiality space. Int. J. Mech. Sci. **46** (1) (2004) pp. 81–98.
9. Behrens A and Westhoff B. - Finite Element Modeling of high speed machining processes. PTW TU Darmstadt (1999) p. 6.
10. Sharif S, Teknologi U, and Universiti I. - High Speed Dry End Milling of Ti-6Al-4V Alloy towards Nano-scale Surface Roughness. Journal of Applied Sciences Research **8** (2012) pp. 4–9.
11. Banh Tien Long, Tran The Luc and Tran Sy Tuy. - Metal Cutting Principles. 2nd Ed (2011). Science and Technics Publishing House.

TÓM TẮT

NGHIÊN CỨU MÔ PHỎNG QUÁ TRÌNH HÌNH THÀNH PHOI KHI PHAY CAO TỐC HỢP KIM NHÔM

Phạm Thị Hoa[1, 2, *], Mạc Thị Bích[1, 2], Bành Tiến Long[1], Nguyễn Đức Toàn[1]

[1]*Khoa Cơ khí, Trường Đại học Sư Phạm Kỹ Thuật Hưng Yên, Xã Dân Tiến, Huyện Khoái Châu, Tỉnh Hưng Yên, Việt Nam*

[2]*Bộ môn GCVL&DCCN, Viện Cơ Khí, Trường Đại học Bách Khoa Hà Nội, Số 1A, Đại Cồ Việt, Quận Hai Bà Trưng, Thành Phố Hà Nội, Việt Nam*

[*]Email*: hoapt2108@gmail.com*

Hiện nay dự đoán cơ chế hình thành phoi và một số các hiện tượng xảy ra trong quá trình cắt bằng mô phỏng đã mang lại một lợi ích rất lớn về kinh tế cũng như tiết kiệm đáng kể về thời gian so với thực nghiệm. Mô phỏng quá trình cắt bằng phương pháp phần tử hữu hạn là một trong phương pháp mô phỏng hiệu quả, chính xác của quá trình cắt. Nghiên cứu này áp dụng phương pháp phần tử hữu hạn cùng với việc phân tích 2 mô hình phá hủy vật liệu của Johson-Cook và Y. Bao –T. Wierzbicki để mô phỏng quá trình hình thành phoi khi phay cao tốc hợp kim nhôm A6061. Đồng thời phân tích sự phân bố ứng suất tương đương Mises và ứng suất biến dạng PEEQ ở các trạng thái mà phoi được hình thành. Nghiên cứu cũng so sánh lực cắt hình thành trong quá trình mô phỏng giữa hai mô hình phá hủy trên. Từ sự phân tích này đưa ra được mô hình phù hợp với mô phỏng quá trình phay nói riêng và mô phỏng quá trình cắt gọt vật liệu nói chung.

Từ khóa: phay cao tốc, hợp kim nhôm A6061, mô phỏng phần tử hữu hạn.